Green Synthesis of Fe_3O_4@CDs Nanocomposites and its Performance on Optical and Magnetic Properties

Astuti
Physics Department, Faculty of Mathematics and Natural Sciences, Andalas University

Arief, Syukri
Chemistry Department, Faculty of Mathematics and Natural Sciences, Andalas University

Muldarisnur, Mulda
Physics Department, Faculty of Mathematics and Natural Sciences, Andalas University

Zulhadjri
Chemistry Department, Faculty of Mathematics and Natural Sciences, Andalas University

https://doi.org/10.5109/7183339

出版情報：Evergreen. 11 (2), pp.673-681, 2024-06. 九州大学グリーンテクノロジー研究教育センター
バージョン：

Green Synthesis of Fe_3O_4@CDs Nanocomposites and its Performance on Optical and Magnetic Properties

Astuti[1], Syukri Arief[2,*], Mulda Muldarisnur[1], Zulhadjri[2]

[1]Physics Department, Faculty of Mathematics and Natural Sciences, Andalas University, Padang, Indonesia.

[2]Chemistry Department, Faculty of Mathematics and Natural Sciences, Andalas University, Padang, Indonesia

E-mail: syukriarief@sci.unand.ac.id

(Received February 2, 2023; Revised February 13, 2024; accepted April 3, 2024).

Abstract: The coprecipitation technique has successfully created iron oxide (Fe_3O_4) nanoparticles. The surface of Fe_3O_4 nanoparticles was then modified with luminescent material, namely carbon dots (CDs). CD was synthesized from dried banana leaves using a simple heating method. Then, the Fe_3O_4@CDs nanocomposite was synthesized using the hydrothermal method of one-pot and two-pot synthesis. The CD is transparent under visible light and looks blue and green under UV illumination. The photoluminescence properties of CDs and Fe_3O_4@CDs nanocomposite were characterized using photoluminescence (PL) spectrophotometers. Fe_3O_4@CD synthesized using a one-pot technique has an emission band that broadens towards longer wavelengths, or "redshift." In contrast, Fe_3O_4@CDs synthesized using a two-pot technique has a higher luminescent intensity than pure CDs. A transmission electron microscopy (TEM) image shows the core-shell structure of the Fe_3O_4@CDs nanocomposite. Vibrating sample magnetometry (VSM) results show that the nanocomposite has a saturation magnetization of 22.3 emu/g and a coercivity field of 85.41 Oe. The functional groups in Fe_3O_4@CDs nanocomposite are Fe-O bonds, indicating the formation of Fe_3O_4, whereas O-H and C=O bonds indicate the formation of CDs. Based on the optical and magnetic characterization, it can be concluded that this material can be developed for a biomedical application, such as a bioimaging material.

Keywords: Nanocomposites, magnetic materials, biocompatibility, carbon dot

1. Introduction

Nanoparticles are nanoscale materials that have different characteristics compared to bulk materials. New properties in these nano-sized particles are applied extensively in the biomedical field, including as the contrast agent for magnetic resonance imaging (MRI), drug delivery systems, and bioimaging[1-4]. Bioimaging materials must possess good magnetic and luminescence properties. Combining nanoparticles with good magnetic and optical properties converted into luminescent, magnetic nanocomposites are appealing to be developed. One of the magnetic nanoparticles commonly used in the biomedical field is Fe_3O_4 nanoparticles due to their size-dependent magnetic properties. Some examples of Fe_3O_4 in biomedical applications are as a therapy for Alzheimer's disease[5], detection of uric acid[6], live cell imaging[7], hyperthermia [8-10], and many others. The smaller the size, the stronger the magnetic response of the Fe_3O_4 nanoparticles[4,11]. Fe_3O_4 is not biocompatible in biomedical applications, so surface modification must be carried out by coating the surface with biocompatible materials. Surface modifications can be done by coating the surface of nanoparticles using core-shell structured organic or inorganic materials[12,14]. The shell material in the core-shell structure minimizes the toxic effects that the core material might generate. Consequently, it is safe to be used as bioimaging material[11].

Some researchers have reported the surface modification of Fe_3O_4 magnetic nanoparticles with luminescence materials[15-17]. One of the luminescent materials that has the potential to be combined with Fe_3O_4 is the carbon dot (CDs). CDs are carbon materials whose size is below 10 nm, showing photoluminescence when radiated using UV light. The CDs is advantageous because of its biocompatibility, photostability, high water solubility, non-toxicity, easy synthesis, and producibility from abundant natural materials[18,19]. CDs has been successfully synthesized from natural resources, for example, from purslane leaves using the hydrothermal method[19], Azadirachta indica leaves[20], lemon peel waste[21], lemon and grapefruit extract[22], and other organic materials by other researchers.

This study synthesized CDs from the waste of dried banana leaves. Dried banana leaves have cellulose, which can be synthesized into carbon[23]. Hence, dried banana leaves can be used as the primary material for CDs. Besides, the advantage of using dried banana leaf waste is

that the synthesis process is straightforward, and its availability is abundant, thereby reducing costs in the CDs synthesis process. Fe_3O_4@CDs was synthesized using the hydrothermal method, using two different techniques: one- and two-pot synthesis. Then, we compare the optical properties using a photoluminescence (PL) and UV-vis spectrometer. The magnetic properties were analyzed using the vibrating sample magnetometer (VSM).

2. Experimental

2.1 Materials and instruments

Materials used in this study were $FeCl_3.6H_2O$ (Merck) and $FeSO_4.7H_2O$ (Merck), NH_4OH 21% (*Bratachem*), and alcohol 96%. The sample's phase and crystal structure were characterized using the X-ray diffractometer (XRD, Bruker D8 Advance). Fourier Transform Infra Red Spectroscopy (FTIR, Nicolet iS50 FTIR) was used to determine the formed chemical bonds. The Vibrating-Sample Magnetometer (VSM, VSM250) and the Photoluminescence (PL, Horiba Micro Photoluminescence Microspectrometer) were used to analyze the magnetic and optical properties of the samples, respectively.

2.2 Synthesis of Fe_3O_4

As much as 8.109 g of $FeCl_3.6H_2O$ and 4.170 g of $FeSO_4.7H_2O$ were dissolved in 30 ml of aquadest (distilled water) while being heated on a hot plate at 60 °C to create Fe_3O_4 nanoparticles using the coprecipitation method. A total of 30 ml of NH_4OH solution was added drop by drop until a black precipitate was formed while stirring with a magnetic stirrer for 90 minutes. A permanent magnet was used to form Fe_3O_4 precipitation. The precipitate was washed three times using aquadest and then dried in an oven at 90 °C for 4 hours. The dried precipitate was then ground to obtain fine Fe_3O_4 powder.

2.3 Synthesis of Carbon Dots

The synthesis of CDs from dried banana leaves was conducted using a simple heating method following these steps: dried banana leaves were heated in an oven at 200 °C for 1 hour to remove the moisture in the dried banana leaves. The dried banana leaves were then mashed using a mortar and pestle until they became powder. The carbonization process of dried banana leaf powder was performed using a furnace at 400 °C for 1 hour; carbon was ground until smooth. As much as 0.3 g of fine carbon powder was dissolved in 20 ml aquadest. The solution was filtered to separate the carbon deposits to produce CDs colloids.

2.4 Synthesis of Fe_3O_4@CDs Nanocomposites

The Fe_3O_4@CDs nanocomposite was synthesized using the hydrothermal method with two different techniques. The first technique is one-pot synthesis; The Fe_3O_4@CDs nanocomposite was synthesized by dissolving Fe^{3+} ($FeCl_3.6H_2O$) and Fe^{2+} ($FeSO_4.7H_2O$) with a molar ratio of 2:1 in 30 ml of distilled water. 30 ml of NH_4OH was added slowly into the solution while stirring and heated at 60 °C for 90 minutes. Then, the carbon solution was added to the Fe_3O_4 solution while stirring using a magnetic stirrer. The mixed solution was put into a Teflon autoclave for the hydrothermal process in the oven at 180 °C for 12 hours. The solution was then sonicated and centrifuged for 20 minutes. The centrifuged precipitate was dried using an oven at 150 °C for 3 hours. The second technique is two-pot synthesis; Fe_3O_4@CDs nanocomposites were synthesized by dissolving 0.4 g of Fe_3O_4 powder in 5 ml of distilled water. Then, as much as 1 g of carbon powder was dissolved in 10 ml of distilled water by adding three drops of isopropanol. The two solutions were mixed and stirred with a magnetic stirrer for 5 minutes. The mixed solution was put into a Teflon autoclave for the hydrothermal process at 180 °C for 12 hours. Then sonicated and centrifuged for 20 minutes. The result of the centrifugation process is in the form of a precipitate and supernatant. The precipitate was dried at 150 °C for 3 hours.

3. Results and discussion

3.1 Colloids of CDs and Fe_3O_4@CDs nanocomposites.

CDs colloids before and after UV irradiation and Fe_3O_4@CDs colloids are shown in Fig 1. Under UV illumination, CDs emit blue light with a high luminescence intensity. CDs and F_3O_4@CDs have high dispersibility in water, and no precipitate was found in the bottom of the container.

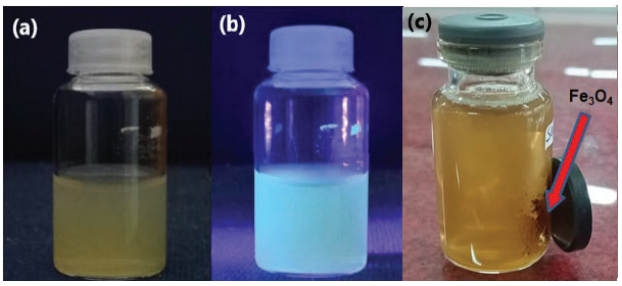

Fig. 1: The colloid of CDs and Fe_3O_4@CDs, (a) CDs before UV illumination, (b) CDs under UV illumination, (c) Magnetic attraction of dispersed Fe_3O_4@CDs toward a magnet.

3.2 Photoluminescence analysis

The photoluminescence properties of CDs and F_3O_4@CDs nanocomposites were measured using a PL spectrometer, shown in Fig 2. Photoluminescence spectra were obtained using an excitation wavelength of 325 nm. The PL broad peak produced by CDs and F_3O_4@CDs nanocomposite is at a wavelength of 350-550 nm. Surface state[24], quantum confinement effect[25], conjugated structures[26], self-trapped excitons[27], edge defects[28], free zigzag sites[29], and multi-emissive centers [30] are the primary fluorescent origins of CDs. CDs has a

photoluminescence peak at 433 nm that emits green luminescence. The absorption above 400 nm originates from the surface state transition with lone electron pairs[31,32].

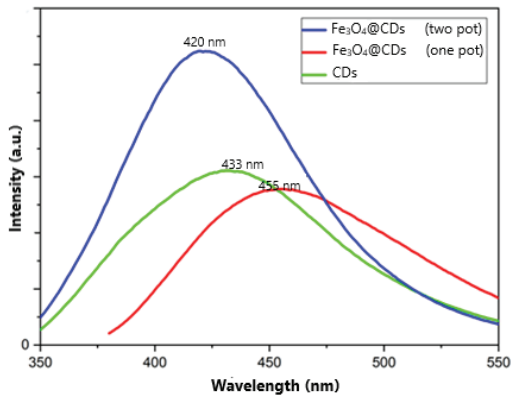

Fig. 2: The PL Spectrum of CDs and Fe_3O_4@CDs nanocomposite

Differences in the synthesis technique of the Fe_3O_4@CDs nanocomposite affect the photoluminescence properties. The broad peak absorption of this sample is similar to CDs, indicating a similar photoluminescence mechanism, i.e., surface state transition with electron lone pairs surface/edge types have a more critical effect on the optical properties of CDs. The slight decrease in emission intensity and wavelength shift towards longer wavelengths in Fe_3O_4@CDs nanocomposite (one-pot synthesis) was influenced by the concentration of Fe_3O_4 precursor solution during the synthesis process. However, the broadening of the emission peak and redshift are observed here. Because of the ensuing nonradiative electron/hole recombination, the fluorescence of CDs quenchs[32]. Fourier transform infrared (FTIR) investigations proved that CDs bound to the iron oxide surface. The Fe_3O_4@CDs composite showed a considerable decrease in the peak intensity of the oxygenated functional groups of CDs, such as −C═O and C–O–C (~1487.42 cm^{-1} and 1106 cm^{-1}), suggesting their participation in surface stabilization.

Furthermore, a new peak at approximately 547.78 cm^{-1} and 459.06 cm^{-1} that is indicative of Fe–O stretching was also detected (Fig. 7). PL spectrum of CDs and Fe_3O_4@CDs nanocomposites (two-pot synthesis), it appears that both have similar PL properties. It should be mentioned that since the Fe_3O_4 nanoparticles are not photoluminescent, the PL of the Fe_3O_4@CDs nanocomposite should originate from the CDs or the contact between the Fe_3O_4 nanoparticles and carbon. Therefore, surface functional groups and surface energy traps that become emissive upon stabilization due to surface passivation may cause the observed luminescence emission. The radiative recombination of excitations is a commonly accepted mechanism for luminescence emission. The high photoluminescence intensity indicates that the electron recombination process occurs quickly in CDs[33].

3.3 UV-Vis analysis

The UV-Vis and photoluminescence spectra of CD can be seen in Fig. 3. The CD UV-Vis spectrum shows an absorption peak in the UV region in the wavelength range of 200–350 nm. There are two absorption peaks with peaks of 240 nm and 308 nm, which are the $\pi \rightarrow \pi^*$ electron transition in the C=C bond in the sp^2 hybridized domain of graphitic core and the $n \rightarrow \pi^*$ electron transition in the C=O bond in the sp^3 hybridized domains, respectively[34,35]. Very bright fluorescence was observed at the emission peak of 433 nm. Based on the absorption spectrum and emission spectrum, it can be explained that there is a relatively large Stokes shift, namely around 125 nm. This significant Stokes shift is likely caused by the strong interaction between the excited dipole moment of the CD and nearby water molecules, and the emission in the CD is thought to be a triplet excitation[36,37].

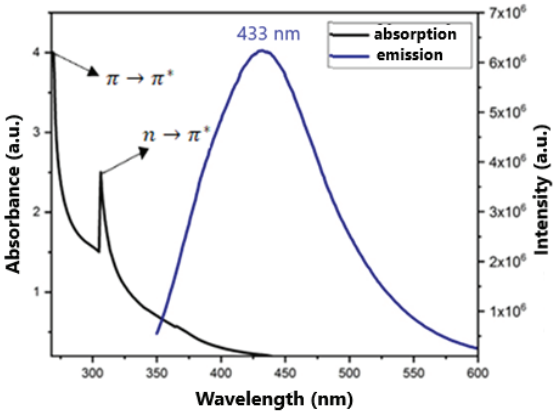

Fig.3. UV-Vis absorption and photoluminescence of CDs

Figure 4 shows the absorbance spectrum of CD and Fe_3O_4@CD nanocomposites. CD and Fe_3O_4@CD nanocomposites have absorbance peaks in the UV region at the 200-350 nm wavelength range. The entire photophysical reactions of CD in light absorption and emission processes are based on a sp^2 carbon backbone-derived isolated network of π-bonding

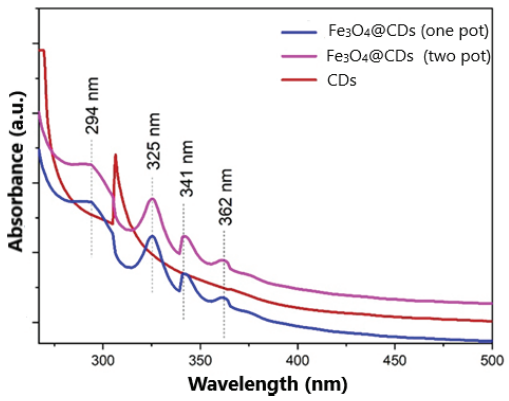

Fig. 4. The absorbance spectrum of Carbon dot and Fe_3O_4@CD nanocomposite

Fe_3O_4@CD nanocomposites show blue-green emission, corresponding to a wavelength of 300–360 nm. The absorbance spectrum of Fe_3O_4@CD nanocomposite, which was synthesized one-pot and two-pot, had four absorbance peaks at the same wavelengths, namely at 294 nm, 325 nm, 341 nm, and 362 nm. The absorbance of Fe_3O_4@CD nanocomposite (one-pot) and Fe_3O_4@CD nanocomposite (two-pot) is lower than the absorbance of CD. The absorbance peaks decreased due to Fe_3O_4 contained in the Fe_3O_4@CD nanocomposite colloid. Fe_3O_4@CD nanocomposite (two-pot) shows a higher absorbance than Fe_3O_4@CD nanocomposite synthesized using the one-pot method. Fe_3O_4@CD (two-pot) nanocomposite has a distinct absorption peak in the ultraviolet region, which is caused by the π–π* transition in the CD [38,39].

3.4 Morphology of Fe_3O_4@CD

TEM is used to determine the morphology of Fe_3O_4@CD more clearly. The TEM image shows that Fe_3O_4@CD (two-pot) size is less than 10 nm. The Fe_3O_4@CD nanocomposite with a core-shell structure diameter of 3-10 nm was obtained (Fig 5 (a)), which can be seen in the particle size distribution histogram in Fig. 5 (c). Our result is similar to those obtained by other researchers[39, 40, 41]. As seen in Fig 5 (b), Fe_3O_4 is the core, while CD envelopes Fe_3O_4 as a shell. In Fig. 5 (b), an image is inserted to determine the interlayer distance in Fe_3O_4, obtaining d_{Fe3O4} = 0.29 nm (Miller index: 220, 2θ= 30.16°), which agrees with the XRD data in Fig. 8.

Based on the SEM image in Fig 6, it can be seen that the Fe_3O_4@CD particles form aggregates from a group of very fine particles. Each particle looks spherical, with an average diameter of 8-20 nm.

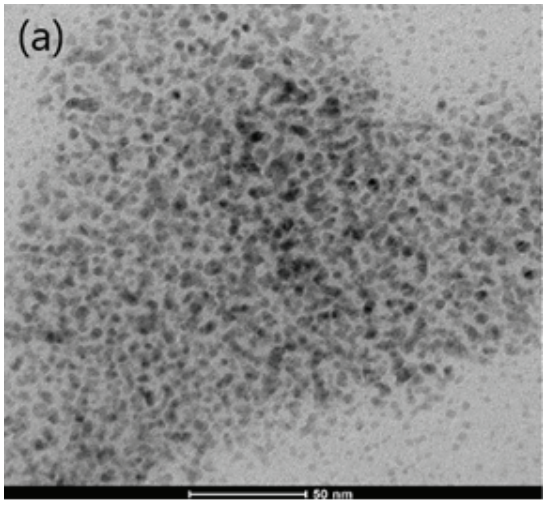

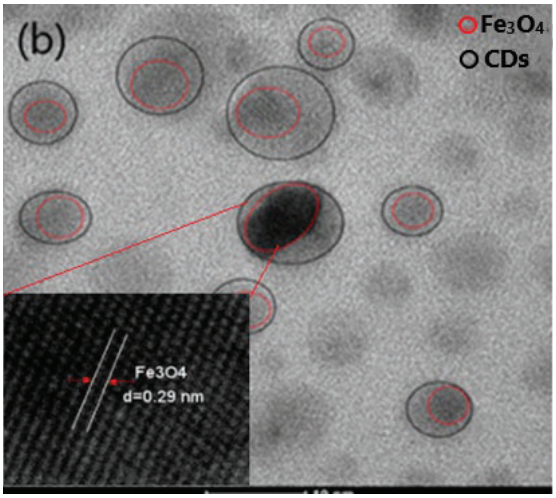

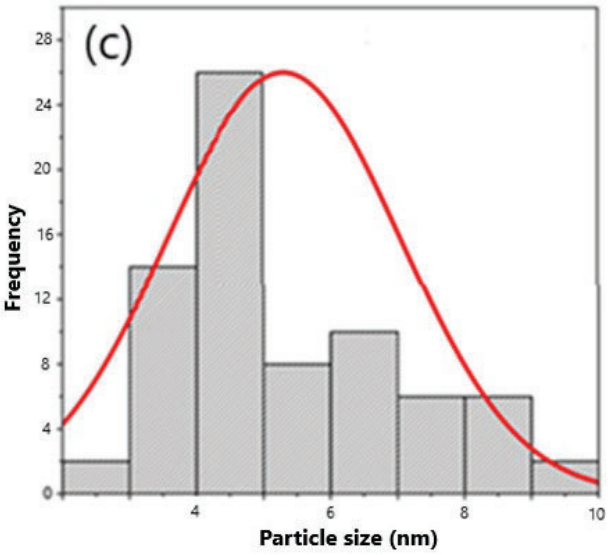

Fig. 5: TEM Image of Fe_3O_4@CD (a) Low ratio, (b) High ratio, (c) Histogram of the particle size distribution of Fe_3O_4@CD.

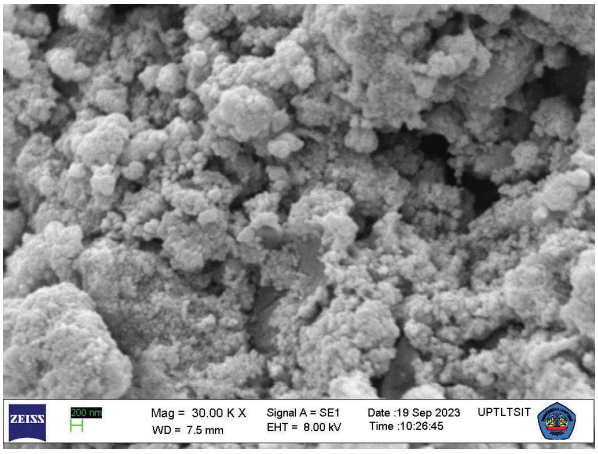

Fig. 6. SEM image of Fe_3O_4@CD

3.5 Functional group of Carbon dot and Fe_3O_4@CD

The results of the functional group analysis on the CD sample and Fe_3O_4@CD nanocomposite are presented in Fig 7. The FTIR spectrum used a wavenumber of 400 – 4000 cm^{-1}. The O-H, C-C, and C=C vibrations are observed for CD around 3292.49 cm^{-1}, 2119.77 cm^{-1}, and 1633.71 cm^{-1}, respectively. The C=C vibration indicated that the CD with a simple heating method had been formed, where the C=C vibration was the primary functional group in CD. Fe_3O_4@CD nanocomposite (one-pot) also observed the O-H stretching at 1487.42 cm^{-1} and the bending absorption of C-O-C at 1106 cm^{-1}. The absorption spectrum indicates the presence of the C-O functional group at a wavenumber of 1203.28 cm^{-1} and the Fe-O functional group at a wavenumber of 547.78 cm^{-1} and 459.06 cm^{-1}.

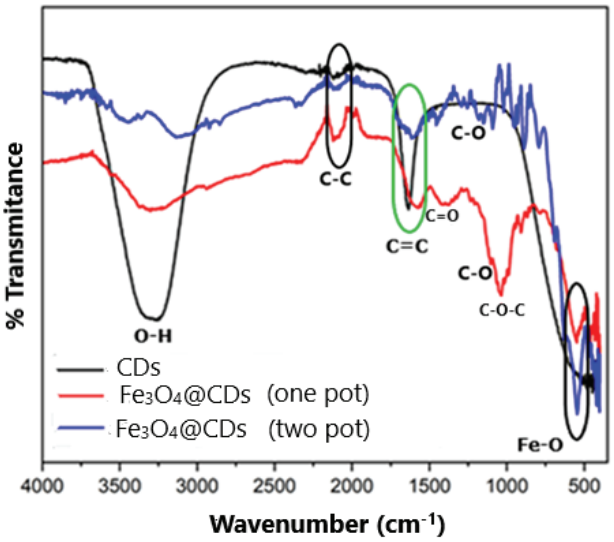

Fig 7. The FTIR spectra of CD, Fe_3O_4@CD (one-pot synthesis), and Fe_3O_4@CD (two-pot synthesis)

The FTIR spectrum of Fe_3O_4@CDs nanocomposite (two-pot) showed the presence of O-H bonds at 3454.51 cm^{-1} and 3116.97 cm^{-1}. The absorption at wavenumber 1606.70 cm^{-1} indicates the presence of the C=C vibration. The bending absorption of C-O was observed at 1149.57 cm^{-1} and 1091.71 cm^{-1}. The absorption at wavenumbers 545.85 cm^{-1} and 478.35 cm^{-1} [42], implying the presence of Fe_3O_4, results from the Fe-O bonds at wavenumbers 400-600 cm^{-1} [17].

3.6 Crystal structure of Carbon dots and Fe_3O_4@CDs nanocomposite

XRD characterization on Fe_3O_4 nanoparticle and Fe_3O_4@CD (two-pot) nanocomposite is presented in Fig 8. XRD patterns of Fe_3O_4 show diffraction peaks with the highest intensity at 2θ = 35.57° with the *hkl* (311), while the other diffraction peaks are at 2θ = 30.16° with the *hkl* (220), 2θ = 43.14° with the *hkl* (400), 2θ = 57.15° with the *hkl* (511), and 2θ = 62.85° with the *hkl* (440). The XRD diffraction peaks indicated similarities to the ICDD No.01-088-0315, the sample formed from the synthesis contains the Fe_3O_4 phase, and the crystal structure of Fe_3O_4 is cubic with lattice parameters $a = b = c$ = 8.3750 Å and = $\beta = \gamma$ = 90°. The observed peaks indicate that the synthesis product was pure Fe_3O_4 without impurities.

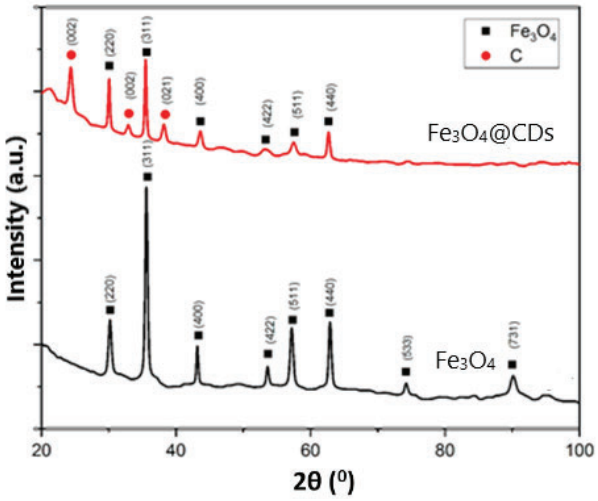

Fig. 8. The XRD patterns of Fe_3O_4 and Fe_3O_4@CD (two pot) nanocomposites

Furthermore, the XRD pattern of the Fe_3O_4@CD nanocomposite showed the presence of carbon peaks at 2θ = 24.3364°, 2θ = 33.4479° and 2θ = 38.1739°. The presence of carbon causes a decrease in diffraction peaks on Fe_3O_4 nanocrystals[43]. The presence of CD was indicated at 2θ = 24.3364°. Based on JCPDS No. 26 -1076, XRD CD pattern produces carbon peaks around 2θ = 20° with *hkl* (002)[44,45]. The crystal size is determined using the Debye-Scherrer equation. The crystal sizes of Fe_3O_4 nanoparticles and Fe_3O_4@CD nanocomposites are 20.39 nm and 27.20 nm, respectively. Based on these calculations, there was an increase in crystal size from 20.39 nm to 27.20 nm. The increase in crystal size was caused by an increase in temperature and reaction time in the hydrothermal process during the synthesis of Fe_3O_4@CD[46].

3.7 Magnetic properties of Fe_3O_4@CD

M-H curves were recorded at room temperature using a vibrating sample magnetometer (VSM). VSM characterization was used to analyze the magnetic properties of Fe_3O_4 and Fe_3O_4@CD nanocomposite shown in Fig. 9. The nanoparticles' magnetic capabilities were reduced after being surface-coated with CD. However, both Fe_3O_4 and Fe_3O_4@CD nanocomposites retained magnetic behavior. Fe_3O_4 M-H curve shows high magnetic saturation (M_s) Oe, i.e., 68.10 emu/g, and a narrow coercivity field (40.22 Oe). However, there is a decrease in M_s (22.30 emu/g) and an increase in H_c (85.41 Oe) of the Fe_3O_4@CD nanocomposite. The presence of CD on the surface of Fe_3O_4 causes a decrease in the magnetic saturation and an increase in the coercivity field of Fe_3O_4@CD nanocomposites that is caused by CD,

which is non-magnetic[44,45]. Higher Hc values are necessary for reverse domain nucleation because smaller particles are less likely to display surface flaws[46].

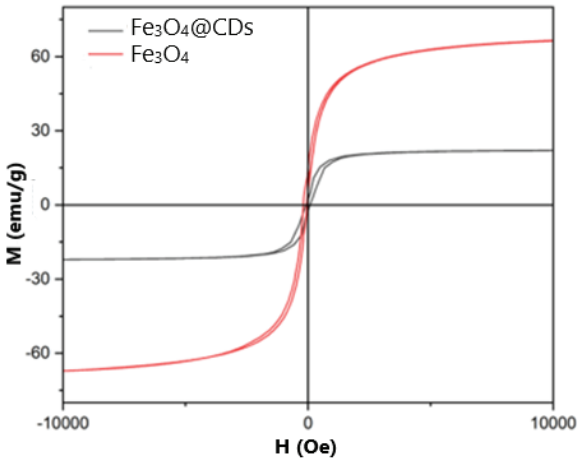

Fig. 9. The hysteresis curve of Fe_3O_4 nanoparticle and Fe_3O_4@CD (two pot) nanocomposite measured at room temperature

The M-H curve on the Fe_3O_4@CD nanocomposite has a narrow area of 0.9 kOe.emu/g. Reduced crystallinity decreases magnetic saturation[47]. However, in biomedical applications, low magnetic saturation values are reported to be better than high saturation values because tissue damage due to high magnetic fields can be minimized[48]. The majority of medical applications typically favor magnetic nanoparticles in the 10–20 nm size range due to their superparamagnetism, low toxicity and agglomeration, high circulation time, improved pharmacokinetics/pharmacodynamics, capacity to diffuse across biological barriers and tissues, and viability of targeting tumors through the enhanced permeability and retentivity (EPR) effect, among other reasons[49]. According to earlier studies, the Ms value of 7–22 emu/g is appropriate for use in biological applications[50,51].

4. Conclusions

The simple heating and hydrothermal methods for synthesizing CD and Fe_3O_4@CD nanocomposite, respectively, were successful. The synthesis of CD from dried banana leaves using a simple heating method was successfully accomplished. Synthesis techniques determine the optical properties of Fe_3O_4@CD nanocomposite. The one-pot synthesis technique shifts the photoluminescent peak to a longer wavelength (redshift). Meanwhile, two-pot synthesis produces higher photoluminescence intensity in the blue emission region. For this reason, the synthesis method and starting materials play an essential role in the optical properties of CD. The saturation magnetization (Ms) of Fe_3O_4@CD nanocomposite 22.30 emu/g. Based on this research, the Fe_3O_4@CD nanocomposite has the potential to be developed as a biomedical material, particularly as a bioimaging material.

Acknowledgements

The research described in this paper was financially supported by Universitas Andalas with research contract number No. 14/UN.16.03.D/PP/FMIPA/2023.

References

1) Mickoleit F and Schüler D (2019) Generation of nanomagnetic biocomposites by genetic engineering of bacterial magnetosomes. *Bioinspired, Biomimetic and Nanobiomaterials* 8(1): 86–98, https://doi.org/10.1680/jbibn.18.00005
2) Rümenapp C, Gleich B and Haase A (2012) Magnetic nanoparticles in magnetic resonance imaging and diagnostic *Pharm. Res,* 29 1165–1179. https://doi.org/10.1007/s11095-012-0711-y
3) G. Rodriguez R, Campbell E, Naumov A, (2019) Multifunctional graphene oxide/ iron oxide nanoparticles for magnetic targeted drug delivery dual magnetic resonance/fluorescence imaging and cancer sensing *PLoS ONE* 14 6 https://doi.org/10.1371/journal.pone.0217072
4) Khosravanian A, Moslehipour A and Ashrafian H, (2021) A review on bioimaging, biosensing, and drug delivery systems based on graphene quantum dots *Prog. Chem. Biochem. Res,* 4 44–56 . https://doi.org/10.22034/pcbr.2020.237134.1102
5) Kuang Y, Zhang J, Xiong M, Zeng W, Lin X, Yi X, Luo Y, Yang M, Li F and Huang Q (2020) A Novel Nanosystem Realizing Curcumin Delivery Based on Fe3O4@Carbon Dots Nanocomposite for Alzheimer's Disease Therapy. Front. Bioeng. Biotechnol. 8:614906. doi: 10.3389/fbioe.2020.614906
6) Malik Waseem Abbas, Razium Ali Soomro, Nazar Hussain Kalwar, Mehvish Zahoor, Ahmet Avci, Erol Pehlivan, Keith Richard Hallam, Magnus Willander, Carbon quantum dot coated Fe3O4 hybrid composites for sensitive electrochemical detection of uric acid, Microchemical Journal, Volume 146, 2019, 517-524, https://doi.org/10.1016/j.microc.2019.01.034.
7) Mohapatra, Sasmita, Sahu, Swagatika, Nayak, Santoshi, Ghosh, Sudip K, 2015 Design of Fe3O4@SiO2@Carbon Quantum Dot Based Nanostructure for Fluorescence Sensing, Magnetic Separation, and Live Cell Imaging of Fluoride Ion, doi: 10.1021/acs.langmuir.5b01513.
8) Yusefi M, Shameli K, Su Yee O, Teow SY, Hedayatnasab Z, Jahangirian H, Webster TJ, Kuča K. Green Synthesis of Fe3O4 Nanoparticles Stabilized by a Garcinia mangostana Fruit Peel Extract for Hyperthermia and Anticancer Activities. *Int J Nanomedicine*. 2021;16:2515-2532 https://doi.org/10.2147/IJN.S284134
9) Vassallo, Marta, Martella, Daniele, Barrera, Gabriele, Celegato, Federica, Coïsson, Marco, Ferrero, Riccardo, Olivetti, Elena S, Troia, Adriano, Sözeri,

Hüseyin, Parmeggiani, Camilla, Wiersma, Diederik S, Tiberto, Paola, Manzin, Alessandra, (2023), Improvement of Hyperthermia Properties of Iron Oxide Nanoparticles by Surface Coating, 8, 2, 2143–2154, https://doi.org/10.1021/acs omega.2c06244

10) A. Hajalilou, L.P. Ferreira, M.E. Melo Jorge, C.P. Reis, M.M. Cruz, (2021), Superparamagnetic Ag-Fe3O4 composites nanoparticles for magnetic fluid hyperthermia, Journal of Magnetism and Magnetic Materials, 537, 168242, https://doi.org/10.1016/j.jmmm.2021. 168242.
11) L. F Fang, M. Xiaoming, S. Jimei, L. Qin, L. Jinliang, (2020) Novel Carbon-Based Magnetic Luminescent Nanocomposites for Multimodal Imaging, *Frontiers in Chemistry*, 8
12) L. Jianhua, K. Lenka, L. Thomas, C. Yohann, S. Johanne, M. Nathalie, E. Tomáš, S. Daniel, R. Eva, and R. Cyrille, (2020) Coating Persistent Luminescence Nanoparticles With Hydrophilic Polymers for in vivo Imaging*, Frontiers in Chemistry,* 8. https://doi.org/10.3389/fchem.2020.584114
13) Abdolrezaei, F, Sabet, M, (2020) In situ green synthesis of highly fluorescent Fe_2O_3@CQD/graphene oxide using hard pistachio shells via the hydrothermal-assisted ballg milling method, *luminescence*, 35: 684– 693https://doi.org/10.1002/bio.3773
14) J. Chen, Z. Guo, H. B. Wang, M. Gong, X. K. Kong, P. Xia, Q. W. Chen, (2013) Multifunctional Fe3O4@C@Ag hybrid nanoparticles as dual modal imaging probes and near-infrared light-responsive drug delivery platform, *Biomaterials*, 34, https://doi.org/10.1016/j.biomaterials.2012.10.002
15) Stachowska J.D, Gamża M.B, Mellor C, Gibbons E.N, Krysmann M.J, Kelarakis A, Gumieniczek-Chłopek E, Strączek T, Kapusta C, and Szwajca A. (2022) Carbon Dots/Iron Oxide Nanoparticles with Tuneable Composition and Properties., *Nanomaterials*. 7, 674. https://doi.org/10.3390/nano12040674
16) Perelshtein I, Perkas N, Rahimipour S, Gedanken A. (2020) Bifunctional Carbon Dots-Magnetic and Fluorescent Hybrid Nanoparticles for Diagnostic Applications, *Nanomaterials*. 16, 1384. https://doi.org/10.3390/nano10071384
17) M. L. Chen, Y. J. He, X.W. Chen, and J.H. Wang (2012) Quantum Dots Conjugated with Fe_3O_4-Filled Carbon Nanotubes for Cancer-Targeted Imaging and Magnetically Guided Drug Delivery, *Langmuir 28,* 47.. https://doi.org/10.1021/la303957y
18) Zhiguo, Sun & Li, Xiaoming & Wu, Ye & Wei, Changting & Zeng, Haibo, (2018) Green luminescence origin of carbon quantum dots: specific luminescence bands originate from oxidized carbon groups, *New Journal of Chemistry*, 42, 10. https://doi.org/10.1039/C7NJ04562J
19) W.A. Amer, A.F. Rehab, M.E. Abdelghafar, N.L. Torad, A.S. Atlam, and MM Ayad, (2019) Green synthesis of carbon quantum dots from purslane leaves for the detection of formaldehyde using quartz crystal microbalance, *Carbon*, 79, 159-171. https://doi.org/10.1016/j.carbon.2021.03.047
20) P.K. Yadav, V.K. Singh, S. Chandra, D. Bano, V. Kumar, M. Talat, and S.H. Hasan, (2019) Green Synthesis of Fluorescent Carbon Quantum Dots from *Azadirachta indica* Leaves and Their Peroxidase-Mimetic Activity for the Detection of H_2O_2 and Ascorbic Acid in Common Fresh Fruits, *ACS Biomaterials Science & Engineering 5*, 623-632. https://doi.org/10.1021/acsbiomaterials.8b01528
21) Tyagi, Ankit & Tripathi, Kumud & Singh, Narendra & Choudhary, Shashank & Gupta, and Raju, (2016) Green synthesis of carbon quantum dots from lemon peel waste: Applications in sensing and photocatalysis*, RSC Adv*, 6. 10. https://doi.org/10.1039/C6RA10488F
22) Fini S.A, Niasari M.F.S and Ghanbari D, (2018) Hydrothermal green synthesis of magnetic Fe_3O_4-carbon dots by lemon and grape fruit extracts and as a photoluminescence sensor for detecting of E. coli bacteria, *Spectrochim. Acta. A. Mol. Biomol. Spectrosc.* 203.. https://doi.org/10.1016/j.saa.2018.06.021
23) Md Palashuddin Sk, Anushree D, (2020) New-generation quantum dots as contrast agent in imaging, *Nanomaterials in Diagnostic Tools and Devices*, 525-556, https://doi.org/10.1016/B978-0-12-817923-9.00018-3.
24) Cui L, Ren X, Sun M, Liu H, Xia L. (2021) Carbon dots: synthesis, properties and applications. *Nanomaterials* (*Basel*). 16, 3419. doi: 10.3390/nano11123419.
25) Jin SH, Kim DH, Jun GH, Hong SH and Jeon S, (2013) Tuning the photoluminescence of graphene quantum dots through the charge transfer effect of functional groups*, ACS Nano*, 7, 2, https://doi.org/10.1021/nn304675g
26) Wang X, Feng Y, Dong P, Huang J, (2019) A mini review on carbon quantum dots: preparation, properties, and electrocatalytic application, *Frontiers in Chemistry*, 7 DOI=10.3389/fchem.2019.00671
27) Cao L, Meziani M J, Sahu S and Sun YP. (2013) Photoluminescence properties of graphene versus other carbon nanomaterials*, Accounts of Chemical Research*, 46, 1. https://doi.org/10.1021/ar300128j
28) Chen W, Li F, Wu C and Guo T, (2014) Optical properties of fluorescent zigzag graphene quantum dots derived from multiwalled carbon nanotubes*, Applied Physics Letters*, 104, 6. https://doi.org/10.1063/1.4863963
29) Ju B, Nie H, Liu Z, Xu H, Li M, Wu C, Wang H and Zhang S. X. A, (2017) Full-colour carbon dots:

integration of multiple emission centers into single particles *Nanoscale*. 9, 35. https://doi.org/10.1039/C7NR04576J

30) Zhu J, Bai X, Bai J, Pan G, Zhu Y, Zhai Y, Shao H, Chen X, Dong B, Zhang H, Song H, (2018) Emitting color tunable carbon dots by adjusting solvent towards light-emitting devices*, Nanotechnology*. 29, 8. DOI 10.1088/1361-6528/aaa321
31) Wang Y, Kalytchuk S, Zhang Y, Shi H, Kershaw S. V and Rogach A L, (2014) Thickness-dependent full-color emission tunability in a flexible carbon dot ionogel, *The Journal of Physical Chemistry Letters*, 5, 8. https://doi.org/10.1021/jz5005335.
32) Majumdar, Biju, Sarma, Dais, Jain, Siddarth. Sarma,Tridib K. (2018), One-Pot Magnetic Iron Oxide–Carbon Nanodot Composite-Catalyzed Cyclooxidative Aqueous Tandem Synthesis of Quinazolinones in the Presence of tert-Butyl Hydroperoxide doi: 10.1021/acsomega.8b01794
33) Sun YP, Zhou B, Lin Y, Wang W, Fernando KA, Pathak P, Meziani MJ, Harruff BA, Wang X, Wang H, Luo PG, Yang H, Kose ME, Chen B, Veca LM, Xie SY. Quantum-sized carbon dots for bright and colorful photoluminescence. J Am Chem Soc. 2006 Jun 21;128(24):7756-7. doi: 10.1021/ja062677d. PMID: 16771487.
34) Holá K, Sudolská M, Kalytchuk S, Nachtigallová D, Rogach A L, Otyepka M and Zbořil, R, (2017) Graphitic nitrogen triggers red fluorescence in carbon dots *ACS Nano*, 11, 12. https://doi.org/10.1021/acsnano.7b06399
35) Sarkar S, Sudolská M, Dubecký M, Reckmeier C J, Rogach A L, Zbořil R and Otyepka M, (2016) Graphitic nitrogen doping in carbon dots causes red-shifted absorption*, Journal of Physical Chemistry C,* 120, 2, https://doi.org/10.1021/acs.jpcc.5b10186
36) Emam, A. N., Loutfy, S. A., Mostafa, A. A., Awad, H., and Mohamed, M. B. (2017). Cyto-toxicity, Biocompatibility and Cellular Response of Carbon Dots-Plasmonic Based Nano-Hybrids for Bioimaging. RSC Adv. 7 (38), 23502–23514. doi:10.1039/c7ra01423f.
37) Azam, Nayab, Najabat Ali, Murtaza, Javaid Khan, Tooba (2021) Carbon Quantum Dots for Biomedical Applications: Review and Analysis, Frontiers in Materials, 2021, 8, https://www.frontiersin.org/articles/10.3389/fmats.2021.700403.
38) Halin D.S.C, Abdullah M.M.B, Razak K.A , Razak M.F.S.A, Ramli M.M, Salleh M.A, V Chobpattana. (2021) The Effect of GO/TiO2 Thin Film During Photodegradation of Methylene Blue Dye Azliza Azani1, Evergreen, 08 (3), 556-564. https://doi.org/10.5109/4491643
39) Magesh Vasanth, Sundramoorthy Ashok K., Ganapathy Dhanraj, Recent Advances on Synthesis and Potential Applications of Carbon Quantum Dots, Frontiers in Materials, 9 2022, https://www.frontiersin.org/articles/10.3389/fmats.2022.906838
40) Wang. H, Wei. Z, Matsui. H, and Zhou. S. (2014) Fe_3O_4/carbon quantum dots hybrid nanoflowers for highly active and recyclable visible-light driven photocatalyst *Journal of Materials Chemistry,* 2. https://doi.org/10.1039/C4TA03130J
41) Borna, S., Sabzi, R.E. & Pirsa, S. Synthesis of carbon quantum dots from apple juice and graphite: investigation of fluorescence and structural properties and use as an electrochemical sensor for measuring Letrozole. J Mater Sci: Mater Electron 32, 10866–10879 (2021). https://doi.org/10.1007/s10854-021-05745-5
42) S. Bance, B. Seebacher, T. Schrefl, L. Exl, M. Winklhofer, G. Hrkac, G. Zimanyi, T. Shoji, M. Yano, N. Sakuma, M. Ito, A. Kato, A. Manabe Grain-size dependent demagnetizing factors in permanent magnets J. Appl. Phys., 116 (2014), pp. 1-18, 10.1063/1.4904854
43) Aprilliani M.N, Rusdiarso B, Trisunaryanti W. (2022) Synthesis of activated carbon-Fe_3O_4 composite as gasoline adsorbent in gasoline-water mixture and its adsorption kinetics study *Evergreen* 09 (3), 701-710, https://doi.org/10.5109/4843101
44) Kim D.W, Kil H.S , Nakabayashi K, Yoon S.H, Miyawaki J (2017) Improvement of electric conductivity of non-graphitizable carbon material via breaking-down and merging of the microdomains, *Evergreen*, 04 (1), 16-20, https://doi.org/10.5109/1808307.
45) Mohamed E, Aki T, Koki M, Hidenobu G, Masatoshi Sakurai, Tsuyoshi Y, Hiroshi N, (2016) Fabrication of ultrananocrystalline diamond/nonhydrogenated amorphous carbon composite films for hard coating by coaxial arc plasma deposition *Evergreen* 03 (1) 1-5 https://doi:10.5109/1657379
46) Sneha Upadhyay, Kinnari Parekh, Brajesh Pandey, (2016) Influence of crystallite size on the magnetic properties of Fe3O4 nanoparticles, Journal of Alloys and Compounds, 678, 478-485, https://doi.org/10.1016/j.jallcom.2016.03.279
47) Ghazanfari, M.R., Kashefi, M., Shams, S.F., and Jaafari, M.R. (2016). Perspective of Fe3O4 nanoparticles role in biomedical applications. *Biochemistry Research International, 2016*, 32 http://dx.doi.org/10.1155/2016/7840161
48) Salem M.L, Gemeay A, Gomaa S, Aldubayan M.A and Assy L, (2020) Superparamagnetic graphene oxide/magnetite nanocomposite delivery system for doxorubicin-induced distinguished tumor cell cycle arrest and apoptosis *J Nanopart Res* 22 219. https://doi.org/10.1007/s11051-020-04932-5.
49) Kritika, Roy, Indrajit, (2022), Therapeutic applications of magnetic nanoparticles: recent advance, Mater.Adv, http://dx.doi.org/

10.1039/D2MA00444E

50) G. Wang, Y. Chang, L. Wang, Z. Wei, J. Kang, L. Sang, X. Dong, G. Chen, H. Wang and M. Qi, *J. Magn. Magn. Mater*., 2013, 340, 57–60.

51) Ming Zhang, Wentao Wang, Yingjun Cui, Xiaohong Chu, Baohong Sun, Ninglin Zhou, Jian Shen, (2018). Magnetofluorescent Fe_3O_4/carbon quantum dots coated single-walled carbon nanotubes as dual-modal targeted imaging and chemo/photodynamic/photothermal triple-modal therapeutic agents, *Chemical Engineering Journal*, 2018, 338, https://doi.org/10.1016/j.cej.2018.01.081.